EUROPEAN ENDODONTIC JOURNAL

ORIGINAL ARTICLE

# Radiomic Parameters in Periapical Lesions: A CBCT Analysis Evaluating Volumetric Size, Cortical Expansion, Erosion, and Shape

**Oscar LOZANO GONZÁLEZ,[1] Marco Felipe SALAS OROZCO,[1] Jaime Trigueros MANCERA,[2] Noé Gustavo MARTÍNEZ CUÉLLAR,[3] Nuria PATIÑO MARÍN[1]**

[1]Department of Clinical Research, Autonomous University of San Luis Potosí, Faculty of Stomatology, San Luis Potosí, México
[2]Department of Endodontics, Latin University, Guanajuato, Mexico
[3]Department of Endodontics, University of Guadalajara, Jalisco, Mexico

## ABSTRACT

**Objective:** To investigate significant differences in selected radiomic parameters when classifying periapical lesions based on volumetric size, cortical expansion, erosion, and shape using Cone Beam Computed Tomography (CBCT).

**Methods:** A retrospective analytical and comparative study was conducted on 100 small field of view (FOV) 50×50 mm CBCT scans collected between the years 2018 and 2023. The study involved qualitative classification of periapical lesions, followed by segmentation and extraction of radiomic parameters. The extracted parameters included first-order features such as energy, entropy, total energy, and uniformity; texture features like grey-level co-occurrence matrix contrast (GLCMC) and neighbouring grey tone difference matrix contrast (NGTDMC); and shape features including elongation, flatness, sphericity, and mesh volume, utilising 3D Slicer and Pyradiomics. The normal distribution of the variables was determined using the Shapiro-Wilk test. Various tests were used to assess significant differences, including Student's t-test, Mann-Whitney U test, ANOVA, and Tukey's post hoc analysis.

**Results:** Significant differences were observed in the following parameters among the classification levels when classifying periapical lesions according to their volumetric size. There were significant differences in energy with a p-value of 0.001 and total energy with a p-value of 0.02. NGTDMC also showed a significant difference with a p-value of 0.001. A larger volumetric size is associated with greater energy and lower contrast. Significant differences in periapical lesions with erosion were found in shape sphericity (mean 0.34, SD 0.10, p=0.01), energy (mean $3.73\times10^{10}$, SD $4.52\times10^{10}$, p=0.002), and NGTDMC (mean 0.05, SD 0.02, p=0.001) compared to lesions without erosion. GLCMC was lower in erosive lesions (mean 18.94, SD 6.81, p=0.03) than in non-erosive ones (mean 22.28, SD 8.48). Regular-shaped periapical lesions demonstrated significantly greater elongation (mean 0.794, SD 0.115, p=0.006) and flatness (mean 0.614, SD 0.107, p=0.005) than irregular-shaped lesions. These findings suggest that regular-shaped periapical lesions are more elongated and flatter than irregular ones. No significant differences were found in radiomic features depending on the presence or absence of expansion in the periapical lesion.

**Conclusion:** There are significant differences in texture and first-order radiomic features in periapical lesions classified based on size, erosion, and shape. This research's relevance lies in its potential to improve the quantitative characterisation of periapical lesions, leading to an objective interpretation.

**Keywords:** CBCT, periapical lesions, radiomics

## HIGHLIGHTS

- Radiomics is an advanced imaging technique that extracts quantitative features from medical images, providing objective and reproducible information about lesion characteristics.
- Radiomic parameters such as energy, NGTDMC, contrast, elongation, and flatness showed significant differences based on lesion size, shape, and erosion, providing insights into the characterisation of periapical lesions.
- Further studies with standardized protocols are essential to validate these findings and expand its clinical applications.

**Please cite this article as:**
Lozano González O, Salas Orozco MF, Mancera JT, Martínez Cuéllar NG, Patiño Marín N. Radiomic Parameters in Periapical Lesions: A CBCT Analysis Evaluating Volumetric Size, Cortical Expansion, Erosion, and Shape. Eur Endod J 2024; 9: 394-404

**Address for correspondence:**
Oscar Lozano Gonzalez
Department of Clinical Research, Autonomous University of San Luis Potosí, Faculty of Stomatology, San Luis Potosí, México
E-mail:
oscarlozanogonzalez@gmail.com

**Received :** November 29, 2023,
**Revised :** February 14, 2024,
**Accepted :** March 24, 2024

**Published online:** December 10, 2024
DOI 10.14744/eej.2024.45220

## INTRODUCTION

Radiology has been indispensable for detecting and characterising periapical lesions in endodontic practice. However, the subjective interpretation of radiographic images can limit the accuracy of diagnosis (1). In recent years, radiomics has emerged as a promising technique for quantitatively evaluating radiographic features and their relationship with pathologies. Radiomics involves the computational analysis of medical images using many features, including texture, shape, and intensity, to obtain objective and quantitative information about image features (2) (Fig. 1). This technique has proven useful in characterising tumours, lung diseases, and other pathologies and has been of growing interest in endodontics (3, 4).

The rise of radiomics has resulted in large amounts of radiographic data forming a solid link with Big Data (5). Progress in artificial intelligence (AI) algorithms and techniques has empowered the management and analysis of these extensive data sets, allowing for a more comprehensive and practical examination of radiomic features and their correlation with different diseases (6). This integration with AI and Big Data has propelled progress in personalised dentistry, allowing treatments to be tailored according to each patient's specific needs based on their radiographic information (7). Radiomics has emerged as a valuable resource in personalised medicine. This approach adjusts treatments and preventive strategies to the unique characteristics of each patient, including their genetic profile, health status, and family history (8). Applying radiomics in personalised dentistry could enable precise identification and characterisation of dental and periapical lesions, facilitating clinical decision-making with objective and quantitative information. This information is essential for predicting treatment response, establishing patient prognosis, improving care quality, and reducing long-term costs. Additionally, radiomics can assist in identifying specific patient subgroups that may benefit from more personalised treatment approaches, leading to better management of oral diseases and increased patient satisfaction (9).

Periapical lesions are prevalent among patients undergoing endodontic treatment, underscoring the importance of accurately characterising them for precise diagnosis and effective treatment planning (10). Traditional radiographic features, while valuable, may need more information to discern the nature of these lesions, highlighting the need for alternative approaches such as radiomics (4). Although the use of radiomics in endodontics has been relatively limited, recent research studies have yielded promising results (11). For instance, a study demonstrated a strong association between the presence of a heterogeneous texture and a periapical cyst, suggesting the potential of radiomics to offer more comprehensive insights into lesion characteristics (12).

Despite its potential benefits, radiomics in endodontics also poses several challenges. One of the main challenges is the need for standardised protocols. There is currently a need for universally accepted protocols for radiomic analysis, which can generate inconsistencies in results and limit the comparability of studies (9). Another challenge is the need for extensive data sets to train and validate radiomic models. Obtaining large datasets of periapical lesions can be challenging due to the low prevalence of these lesions (13). Since radiomics is a promising technique for characterising periapical lesions in endodontics, it has the potential to provide more accurate and objective information about lesion features, improving the accuracy of diagnosis and treatment planning (14). The present study aims to determine whether a significant difference exists between selected radiomic parameters when dividing periapical lesions according to their volumetric size, cortical expansion, cortical erosion, and shape.

## MATERIALS AND METHODS

This was a retrospective analytical comparative study of 100 small field of view (FOV) 50×50 mm CBCT scans. It was conducted using the database of a private dental imaging centre, and patient authorisation was obtained for the development of the study. All ethical guidelines were followed, and informed consent was obtained from the involved patients. Before utilising the patients' data, confidentiality and privacy of the information were ensured.

### Selection Criteria for Computed Tomography

The sampling method used was convenience sampling based on the CBCTs that met the inclusion and exclusion criteria within the established period. The inclusion criteria were images from small FOV CBCT scans of patients with apical lesions between the years 2018–2023, CBCTs of both healthy males and females, patients over 18 years old with no upper age limit, and the periapical lesion should involve only one root of the tooth, whether it is an anterior or posterior tooth. The exclusion criteria were images of patients with diseases that alter bone metabolism (e.g. diabetes, osteopenia, and osteoporosis) and pregnant patients. Images in which the lesion and the surrounding healthy bone tissue could not be fully observed, images with the presence of metal or motion artefacts, lesions involving more than one root or different teeth, and lesions in the presence of root canal treatments carried out in less than one year and without symptoms. Patients under treatment with bisphosphonates were excluded. Images in which the lesions could not be satisfactorily segmented due to a lack of distinction in their edges (Fig. 2).

### Computed Tomography Acquisition Protocol

A Planmeca Promax Classic cone-beam computed tomography scanner was used for all patients, employing a uniform imaging protocol that included a tube voltage of 90 kV, a milliamperage of 10 mA, and a small field of view of 50×50 mm with a resolution of 0.75 microns. A 50-inch LED (Light Emitting Diode) monitor was utilised for image analysis.

### Analysis of Qualitative Parameters of Computed Tomography

Two experts analysed the CBCT scans, each specialising in oral and maxillofacial radiology and endodontics. A qualitative classification examined aspects such as shape, corticalisation, cortical expansion, cortical erosion, and volumetric size of the lesions. The analysis included assessing the lesion's shape and determining if it had a regular or irregular appear-

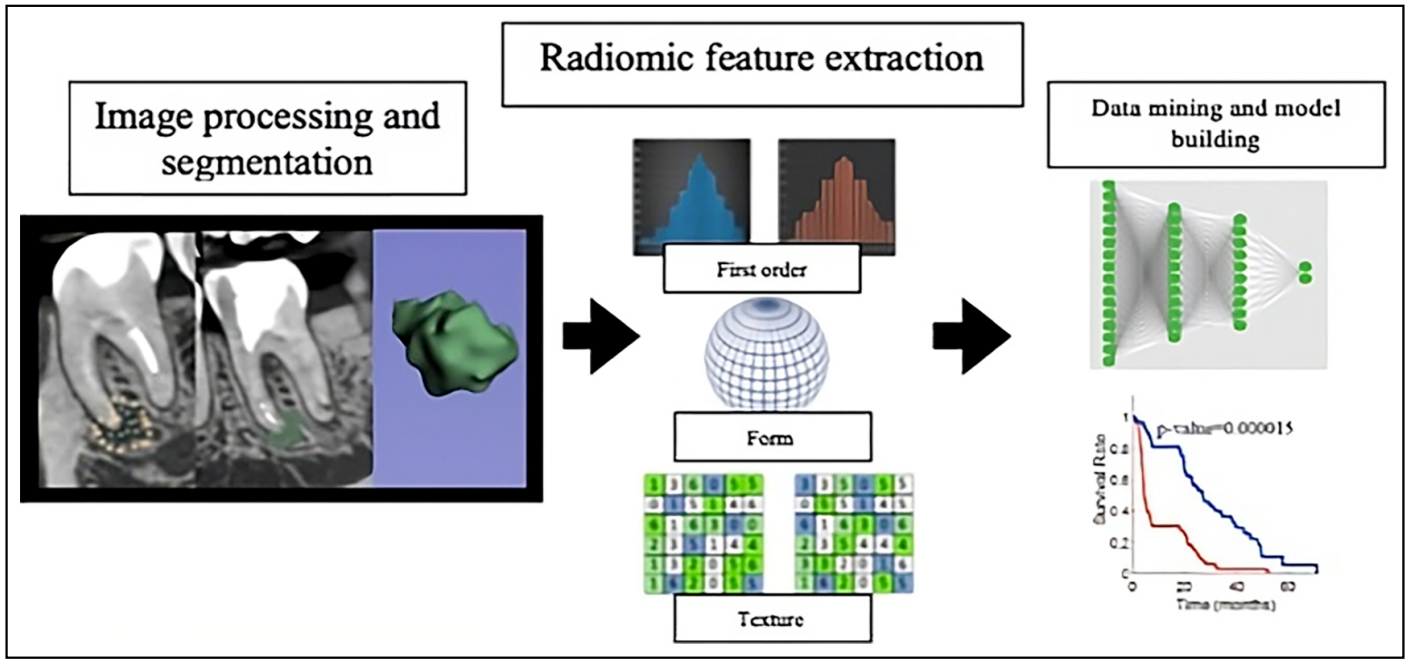


**Figure 1.** Flow diagram for the extraction of radiomic features

**Figure 2.** Non-segmentable periapical lesion of the lower left second premolar due to indistinct border delineation. This image depicts a CBCT scan excluded from the radiomic analysis due to an indistinct periapical lesion that merged with the adjacent mesial root lesion of the lower left first molar, thus impeding precise segmentation

CBCT: Cone Beam Computed Tomography

ance; regular lesions were those with defined borders, symmetrical and easily identifiable, while irregular ones lacked delimited borders. The cortical expansion was classified as present or absent, determined by observing an increase in dimensions of the vestibular or lingual cortices; erosion was evaluated according to whether the apical lesion caused a discontinuity in any of the cortical bones. Finally, corticalisation refers to the characteristics of the edges of the lesion, specifically whether they present a radiopaque halo.

**Volumetric Analysis of Computed Tomography**

Volumetric analysis of the lesions was conducted using conventional CBCT software (Romexis Viewer, Planmeca Oy, Helsinki, Finland). Initially, the scans were imported into the software, and the volumetric analysis tool was selected. Subsequent steps involved delineating regions of interest (ROI) around each lesion by manually tracing their contours in the tomographic images. The software then automatically calculated the volume of the lesions based on these delineated

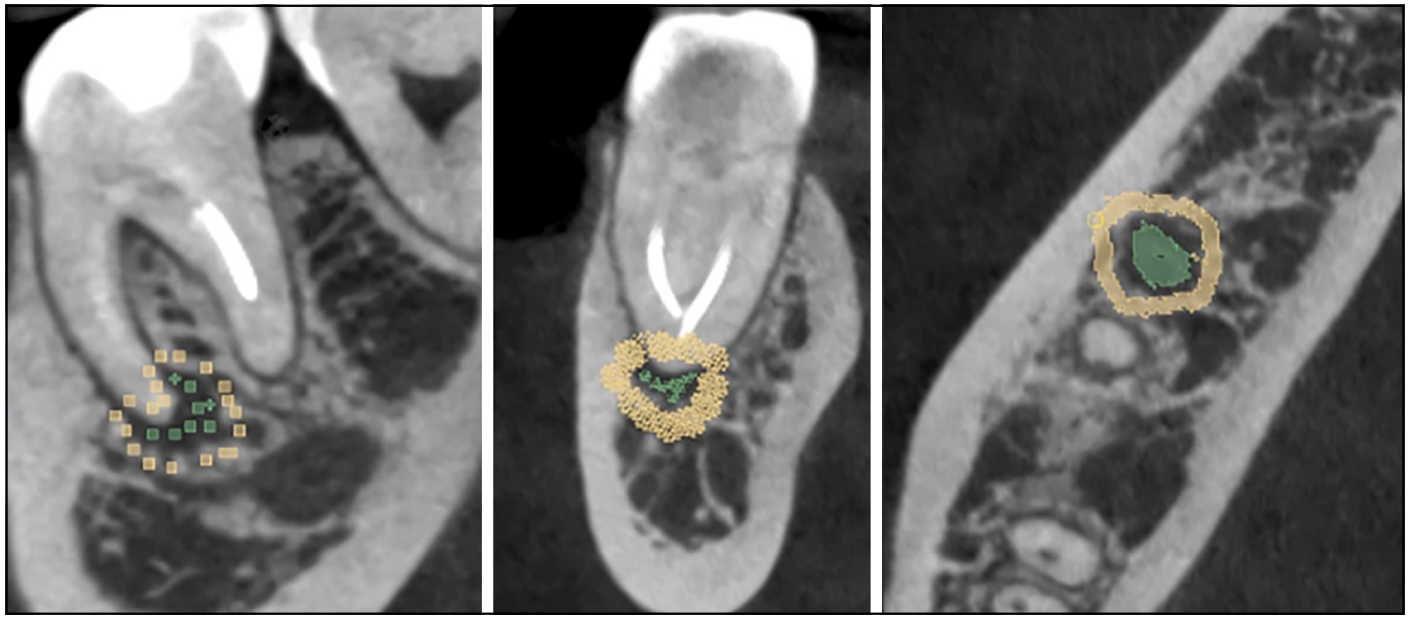

**Figure 3.** Semi-automatic segmentation process using grow from seeds tool in 3D Slicer. Marks are placed on segment 1 (apical lesion-green) in different planes and subsequently on segment 2 (yellow), which will be done on the surrounding bone tissue

ROIs. The volume values obtained for each lesion were meticulously recorded in the study's database. Upon completing the analysis, the classification system proposed by Boubaris in 2021 was employed to categorise the volume of the periapical lesions into six categories ranging from smallest (category 0) to largest volume (category 6) using a novel cone-beam computed tomographic volume-based periapical index (15):

0. 0
1. 0.01 $mm^3$ – 0.20 $mm^3$
2. 0.21 $mm^3$ – 0.70 $mm^3$
3. 0.71 $mm^3$ – 8.00 $mm^3$
4. 8.01 $mm^3$ – 70.00 $mm^3$
5. 70.01 $mm^3$ – 100.00 $mm^3$
6. >100.01 mm

**Analysis of Segmentation and Extraction of Radiomic Parameters from the CBCT Scans**

The voxel resampling method, commonly called resample voxel, was utilised within the open-source software Pyradiomics for standardising image quality across CBCT scans before conducting the radiomic analysis. This preliminary step involved loading the images into Pyradiomics. The voxel resampling technique was then applied, adjusting all voxels to a predefined uniform size and spacing. This standardisation ensures image quality consistency, facilitating more accurate and reliable radiomic analysis (16).

For segmentation and radiomic analysis, 3D Slicer software (developed at the National Biomedical Engineering Laboratory, Boston, Massachusetts, USA) was employed, integrated with the Pyradiomics module (Harvard, Cambridge, Massachusetts, USA) to harness the strengths of both tools in processing medical imaging data. The segmentation was facilitated by a semi-automatic method called grow from seeds. This approach involves initially placing seeds within the anatomical structure targeted for segmentation. Utilising these seeds, the grow from seeds tool within 3D Slicer applies advanced mathematical algorithms to extrapolate and complete the segmentation process, leveraging artificial intelligence and image processing technologies to accurately differentiate and delineate complex structures in medical images (Fig. 3).

3D Slicer's grow from seeds tool is an advanced semi-automatic segmentation technique that uses artificial intelligence and image processing algorithms to differentiate and segment complex structures in medical images. The segmentation process was performed by an experienced oral and maxillofacial radiologist as follows:

1. Seed Initialisation: The process begins with manually placing seeds in the 3D image. Based on their knowledge and analysis of the image, these seeds are small volumes of pixels that the operator assigns to different structures or tissues. For example, in this study, seeds were placed within periapical lesions and in areas of normal bone tissue.

2. Intensity and Texture Analysis: The tool then analyses these seeds intensity and texture characteristics. It uses this information to discern how periapical lesions differ from bone trabeculae and other tissues. This is based on the premise that different tissues exhibit distinct signatures regarding pixel intensity and texture patterns in medical images.

3. Characteristic-Based Growth: With this information, the tool begins the 'growing' process of the seeds. This is not a simple proximity-based space-filling but rather a feature-driven process. The algorithm expands the seeds into areas with similar characteristics in terms of intensity and texture. This ensures the segmentation accurately follows the lesions' boundaries, avoiding including unrelated structures such as bone trabeculae.

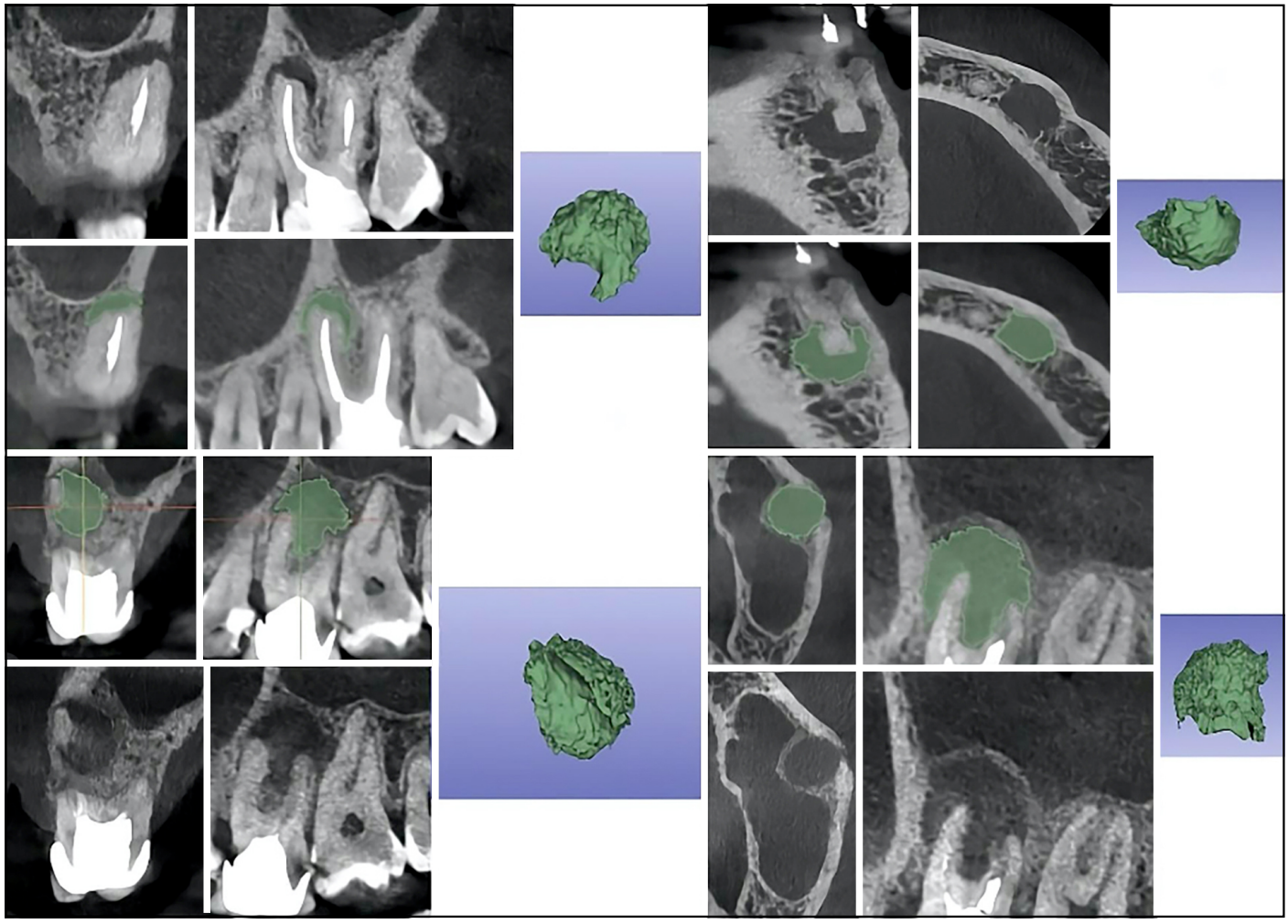

**Figure 4.** Pre- and post-segmentation imaging of periapical lesions utilising 3D Slicer software is demonstrated. The upper multiplanar reconstruction images reveal a CBCT scan with periapical lesions before segmentation. The lower multiplanar reconstruction images exhibit the lesions post-segmentation process (outlined in green). The image on the right shows a 3D reconstruction, accentuating the lesion's detailed topography

CBCT: Cone Beam Computed Tomography

4. Manual Iteration and Adjustment: User interaction is permitted for adjustments during this process. This is crucial in areas where automatic segmentation can be challenging, such as at boundaries where lesions merge with bone spaces. Users can refine the segmentation by adding, moving, or deleting seeds to ensure accurate lesion representation.

5. Completion and Verification: Once the user is satisfied with the segmentation, the process is completed. Previous studies have used and validated this methodology (17, 18) (Fig. 4).

Once the lesion was segmented, radiomic analysis was performed using the Pyradiomics module. This process involved selecting the region of interest previously segmented, extracting radiomic features from ROI, and choosing, in this case, features related to shape, first-order features, and texture, which were selected based on previous articles.

Radiomic shape parameters evaluated were:

- Elongation: It is a measure that describes the relationship between the two most significant main components in the shape of an ROI, and for calculation purposes, it is defined as the inverse of the actual elongation.

- Flatness: It describes the relationship between the largest main component and the smallest in the shape of an ROI, and for calculation purposes, it is defined as the inverse of the actual flatness.

- Sphericity: It is a dimensionless measure that evaluates the roundness of the shape of the tumour region in relation to a sphere. A value of 1 represents a perfect sphere with the smallest surface area compared to other solids.

- Mesh volume: It is calculated using the triangular mesh. For each face on the mesh, the volume of the tetrahedron formed by the face and the image's origin is determined.

Radiomic texture parameters analysed were:

- Gray-Level Co-Occurrence Matrix Contrast (GLCMC): It measures the intensity variation in an image, and a higher value indicates a more significant difference in intensity values between neighbouring voxels.

**TABLE 1.** Classification of periapical lesions according to their volumetric size

| Classification | Range ($mm^3$) | n |
|---|---|---|
| Class 1 | 0.01 $mm^3 \leq \times < 0.20$ $mm^3$ | 2 |
| Class 2 | 0.21 $mm^3 \leq \times < 0.70$ $mm^3$ | 9 |
| Class 3 | 0.71 $mm^3 \leq \times < 8.00$ $mm^3$ | 31 |
| Class 4 | 8.01 $mm^3 \leq \times < 70.00$ $mm^3$ | 49 |
| Class 5 | 70.01 $mm^3 \leq \times < 100.00$ $mm^3$ | 9 |

- Neighbouring Gray Tone Difference Matrix Contrast (NGTDMC): It evaluates the spatial intensity variation in an image, which depends on the dynamic range of grey levels and the speed at which intensity values change between voxels and their surrounding areas.

The first-order radiomic parameters analysed were:

- Energy: Energy measures the magnitude of the values (grayscale) of the voxels in an image, and larger values indicate a more significant sum of the squares of these values.
- Entropy: Entropy refers to the uncertainty or randomness in the values of an image and calculates the average amount of information required to encode these values.
- Total Energy: This measure represents the energy-adjusted according to the voxel volume, considering the size in cubic millimetres.
- Uniformity: It evaluates the homogeneity of the image matrix based on the sum of the squares of each intensity value. Greater uniformity in the image indicates greater homogeneity and a smaller range of discrete intensity values.

Subsequently, the CBCTs were divided into groups according to the previously evaluated qualitative characteristics of the periapical lesions, which were (Table 1-4):

- Presence or absence of erosion
- Shape of the periapical lesion
- Presence or absence of cortical expansion
- Volumetric size category

After selecting the images based on the previously mentioned qualitative criteria, control groups were meticulously formed according to the characteristics of the analysed periapical lesions. For example, from the initial selection of 100 images, 33 were identified to have periapical lesions with an irregular

**TABLE 2.** ANOVA to compare the volumetric size of the periapical lesion with the radiomic characteristics

**Radiomic shape parameters**

| | | Shape_Elongation | | | Shape_Flatness | | | Shape_MeshVolume | | | Shape_Sphericity | | |
|---|---|---|---|---|---|---|---|---|---|---|---|---|---|
| Class | n | Mean | SD | p | Mean | SD | p | Mean | SD | p | Mean | SD | p |
| 1 | 2 | 0.89 | 0.13 | 0.26 | 0.65 | 0.08 | 0.56 | 26.51 | 17.14 | 0.97 | 0.46 | 0.04 | 0.11 |
| 2 | 9 | 0.72 | 0.16 | | 0.54 | 0.15 | | 25185.57 | 64648.83 | | 0.38 | 0.08 | |
| 3 | 31 | 0.75 | 0.14 | | 0.56 | 0.12 | | $5.54\times10^{12}$ | $2.93\times10^{13}$ | | 0.36 | 0.12 | |
| 4 | 49 | 0.72 | 0.14 | | 0.57 | 0.13 | | $4.28\times10^{12}$ | $3.00\times10^{13}$ | | 0.35 | 0.1 | |
| 5 | 9 | 0.79 | 0.06 | | 0.62 | 0.13 | | $6.80\times10^{7}$ | $2.04\times10^{8}$ | | 0.28 | 0.09 | |

**First order radiomic parameters**

| | | Firstorder_Energy | | | Firstorder_Entropy | | | Firstorder_TotalEnergy | | | Firstorder_Uniformity | | |
|---|---|---|---|---|---|---|---|---|---|---|---|---|---|
| Class | n | Mean | SD | p | Mean | SD | p | Mean | SD | p | Mean | SD | p |
| 1 | 2 | $5\times10^{8}$ | $2.50\times10^{8}$ | 0.001* | 5.06 | 0.2 | 0.98 | $1.82\times10^{6}$ | 844528.58 | 0.02* | 0.04 | $7.21\times10^{-3}$ | 0.26 |
| 2 | 9 | $6\times10^{9}$ | $1.02\times10^{10}$ | | 4.93 | 0.32 | | $4.34\times10^{9}$ | $1.07\times10^{10}$ | | 0.04 | $8.97\times10^{-3}$ | |
| 3 | 31 | $1\times10^{10}$ | $1.54\times10^{10}$ | | 4.96 | 0.35 | | $1.19\times10^{9}$ | $4.98\times10^{9}$ | | 0.04 | $9.34\times10^{-3}$ | |
| 4 | 49 | $3\times10^{10}$ | $2.81\times10^{10}$ | | 4.95 | 0.27 | | $4.14\times10^{9}$ | $1.11\times10^{10}$ | | 0.04 | $8.23\times10^{-3}$ | |
| 5 | 9 | $1\times10^{11}$ | $5.87\times10^{10}$ | | 4.92 | 0.29 | | $2.24\times10^{10}$ | $4.47\times10^{10}$ | | 0.04 | 0.01 | |

**Radiomic texture parameters**

| | | Texture_ GLCMC | | | Texture_ NGTDMC | | |
|---|---|---|---|---|---|---|---|
| Class | n | Mean | SD | p | Mean | SD | p |
| 1 | 2 | 33.46 | 0.65 | 0.06 | 0.12 | 0.05 | 0.001* |
| 2 | 9 | 20.73 | 5.48 | 0.08 | 0.02 | | |
| 3 | 31 | 21.24 | 7.81 | 0.07 | 0.03 | | |
| 4 | 49 | 19.81 | 7.89 | 0.05 | 0.02 | | |
| 5 | 9 | 16.33 | 6.68 | 0.03 | 0.01 | | |

*: $p<0.05$. n: Number, SD: Standard deviation

**TABLE 3.** Post-hoc comparisons – Volumetric size and selected radiomic characteristics

| NGTDMC | | | Energy | | | Total energy | | |
|---|---|---|---|---|---|---|---|---|
| **Class (mean)** | **Comparison (mean)** | **p** | **Class (mean)** | **Comparison (mean)** | **p** | **Class (mean)** | **Comparison (mean)** | **p** |
| 1 (0.12) | 1 (0.12) | 0.2 | 1 ($5.41\times10^{8}$) | 1 ($5.41\times10^{8}$) | 1 | 1 ($1.82\times10^{6}$) | 1 ($1.82\times10^{6}$) | 0.997 |
| | 2 (0.08) | <0.05* | | 2 ($5.71\times10^{9}$) | 1 | | 2 ($4.34\times10^{9}$) | 1 |
| | 3 (0.07) | <0.001* | | 3 ($1.16\times10^{10}$) | 0.6 | | 3 ($1.19\times10^{9}$) | 0.996 |
| | 4 (0.05) | <0.001* | | 4 ($2.97\times10^{10}$) | <0.001* | | 4 (0.05) | 0.374 |
| 2 (0.08) | 3 (0.07) | 0.3 | 2 ($5.71\times10^{9}$) | 3 ($1.16\times10^{10}$) | 1 | 2 ($4.34\times10^{9}$) | 3 ($1.19\times10^{9}$) | 0.985 |
| | 4 (0.05) | <0.05* | | 4 ($2.97\times10^{10}$) | 0.1 | | 4 ($4.14\times10^{9}$) | 1 |
| | 5 (0.03) | <0.01* | | 5 ($1.13\times10^{11}$) | <0.001* | | 5 ($2.25\times10^{10}$) | 0.119 |
| 3 (0.07) | 4 (0.05) | 0.056 | 3 ($1.16\times10^{10}$) | 4 ($2.97\times10^{10}$) | <0.05* | 3 ($1.19\times10^{9}$) | 4 ($4.14\times10^{9}$) | 0.927 |
| | 5 (0.03) | <0.01* | | 5 ($1.13\times10^{11}$) | <0.001* | | 5 ($2.25\times10^{10}$) | 0.006* |
| 4 (0.05) | 5 (0.03) | 0.076 | 4 ($2.97\times10^{10}$) | 5 ($1.13\times10^{11}$) | <0.001* | 4 ($4.14\times10^{9}$) | 5 ($2.25\times10^{10}$) | 0.017* |

*: p<0.05. NGTDMC: Neighbouring grey tone difference matrix contrast, n: Number, SD: Standard deviation

**TABLE 4.** Descriptive statistics of patients according to the qualitative variables of the periapical lesion

| | | | | Age | |
|---|---|---|---|---|---|
| **Variable** | **Sex** | **n** | **Total (n)** | **Mean** | **SD** |
| Erosion | Male | 25 | 55 | 45.3 | 15 |
| | Female | 30 | | 45.9 | 11.8 |
| No erosion | Male | 14 | 45 | 49.5 | 11.9 |
| | Female | 31 | | 46.8 | 11.6 |
| Irregular shape | Male | 13 | 33 | 47.2 | 12.7 |
| | Female | 20 | | 47.8 | 9.5 |
| Regular shape | Male | 12 | 33 | 48.3 | 11.9 |
| | Female | 21 | | 46.5 | 9.4 |
| Expand | Male | 7 | 15 | 50.7 | 14.7 |
| | Female | 8 | | 50.5 | 7.2 |
| Does not expand | Male | 7 | 15 | 49.9 | 11.9 |
| | Female | 8 | | 50.7 | 9.4 |

*: p<0.05. n: Number, SD: Standard deviation

shape. Subsequently, from the remaining 67 images, another 33 were selected, which had regular-shaped periapical lesions to establish a control group. This selection was carefully made to ensure a similar age range and gender distribution between the control group and the group with irregularly shaped lesions, thereby aiming to minimise confounding variables. This systematic approach was consistently applied to other qualitative characteristics of the periapical lesions, ensuring that each control group accurately mirrored the specific feature being analysed in the study group.

### Statistical Analysis

The Shapiro-Wilk test was used to determine the distribution of the data. Quantitative variables will be reported through the mean and standard deviation. Qualitative variables will be reported through frequencies or percentages. To identify significant differences between two groups of quantitative radiomic variables, the student's t-test or Mann-Whitney U test was used, depending on the data distribution. An analysis of variance (ANOVA) and post hoc Tukey tests were performed to determine significant differences when there were more than two groups. For the determination of the intra- and inter-agreement between evaluators, Cohen's kappa coefficient was used for qualitative and quantitative variables; the intraclass correlation index was used. A significance level of p<0.05 was used. All statistical analyses were performed using the IBM SPSS STATISTICS 27 software.

## RESULTS

In the study, 100 CBCT scans with a small field of view met the inclusion criteria within the specified timeframe, and 13 CBCT scans were excluded. Among these, 39 were from male patients and 61 from female patients. The mean age for male participants was 46.7 years, ranging from 28 to 73 years, while the mean age for female participants was 46.3 years, ranging from 18 to 82 years. Each of the 100 CBCT scans analysed featured a single tooth: 12 anterior teeth, 5 canines, 16 premolars, and 73 molars. The results of the intra- and inter-reliability assessments measured by Cohen's kappa coefficient indicated a level of agreement around 0.70, which is considered an acceptable level of consistency for this study.

### Difference in Radiomic Parameters according to the Volumetric Size of the Periapical Lesion

Regarding the analysis of the significant difference in radiomic parameters based on the volumetric size of the periapical lesion, the 100 images were analysed, and the reported frequency of each category is presented in Table 1. According to the findings, most lesions fell into class 4, followed by lesions classified as class 3.

### Difference in Shape Radiomic Parameters according to the Volumetric Size of the Periapical Lesion

No significant differences were found in the shape radiomic parameters (elongation, flatness, sphericity, and mesh volume) and the volumetric size of the periapical lesion (Table 2).

### Difference in Texture Radiomic Parameters according to the Volumetric Size of the Periapical Lesion

Regarding texture radiomic features (GLCMC and NGTDMC) concerning the volumetric size of the lesion, only a significant difference was found in the NGTDMC feature (Table 2). The results indicate that the larger the volumetric size, the less contrast (Table 3).

**TABLE 5.** Difference of the radiomic parameters evaluated according to the presence or absence of erosion

| Parameter | Erosion | n | Mean | SD | test | p |
|---|---|---|---|---|---|---|
| Shape_Elongation | Yes | 54 | 0.74 | 0.14 | Student t | 0.96 |
| | No | 44 | 0.74 | 0.13 | | |
| Shape_Flatness | Yes | 54 | 0.58 | 0.14 | Student t | 0.53 |
| | No | 44 | 0.56 | 0.12 | | |
| Shape_MeshVolume | Yes | 54 | 43389.18 | 136946.85 | Mann-Whitney | 0.09 |
| | No | 41 | $8.90\times10^{12}$ | $4.03\times10^{13}$ | | |
| Shape_Sphericity | Yes | 54 | 0.34 | 0.1 | Mann-Whitney | 0.01* |
| | No | 44 | 0.38 | 0.1 | | |
| Firstorder_Energy | Yes | 54 | $3.73\times10^{10}$ | $4.52\times10^{10}$ | Mann-Whitney | 0.002* |
| | No | 44 | $1.71\times10^{10}$ | $2.45\times10^{10}$ | | |
| Firstorder_Entropy | Yes | 54 | 4.99 | 0.3 | Student t | 0.18 |
| | No | 44 | 4.91 | 0.3 | | |
| Firstorder_TotalEnergy | Yes | 54 | $5.30\times10^{9}$ | $1.59\times10^{9}$ | Mann-Whitney | 0.17 |
| | No | 43 | $4.41\times10^{9}$ | $1.77\times10^{9}$ | | |
| Firstorder_Uniformity | Yes | 54 | 0.04 | $8.97\times10^{-3}$ | Mann-Whitney | 0.07 |
| | No | 44 | 0.04 | $8.46\times10^{-3}$ | | |
| Texture_GLCM Contrast | Yes | 54 | 18.94 | 6.81 | Mann-Whitney | 0.03 |
| | No | 44 | 22.28 | 8.48 | | |
| Texture_ NGTDMC | Yes | 53 | 0.05 | 0.02 | Mann-Whitney | 0.001* |
| | No | 44 | 0.07 | 0.03 | | |

*: $p<0.05$. n: Number, SD: Standard deviation, GLCM: Grey-level co- occurrence matrix, NGTDMC: Neighbouring grey tone difference matrix contrast

**Difference in First-order Radiomic Parameters according to the Volumetric Size of the Periapical Lesion**

Regarding first-order radiomic features (energy, total energy, entropy, and uniformity), a significant difference was found in the energy and total energy parameters (Table 2). The results indicate that the larger the size, the greater the energy (Table 3).

**Difference in Radiomic Parameters according to the Presence or Absence of Erosion in the Periapical Lesion**

The 100 scans with a reduced field of view were classified based on the presence or absence of erosion in the periapical lesions. Fifty-five lesions showed erosion; 25 were males, and 30 were females. Fifty-five images did not show erosion; 14 of these images were of males, and 31 were of females (Table 4). Table 4 shows that the age ranges for males and females are similar.

**Difference in Shape Features according to the Presence or Absence of Erosion in the Periapical Lesion**

A significant difference was only found in the shape parameter of sphericity according to the presence or absence of erosion in the periapical lesion. The results indicate that erosive lesions have lower sphericity (Table 4, 5).

**Difference in Texture Parameters according to the Presence or Absence of Erosion in the Periapical Lesion**

A significant difference was found in both texture parameters (GLCMC and NGTDMC) according to the presence or absence of erosion in the periapical lesion. The results indicate that erosive lesions have lower contrast (Table 4, 5).

**Difference in First-order Parameters according to the Presence or Absence of Erosion in the Periapical Lesion**

A significant difference was only found in the first-order energy parameter according to the presence or absence of erosion in the periapical lesion. The results indicate that erosive lesions have higher energy (Table 4, 5).

**Difference in Radiomic Features according to the Shape of the Periapical Lesion**

Thirty-three images were identified in which the periapical lesion had an irregular shape. Another 33 images with regular-shaped lesions were selected as a control group, matching the proportion of males and females and the age range of the initial images (Table 4). Regarding the differences in selected radiomic parameters based on the shape of the periapical lesion, a significant difference was found only in the shape parameters: elongation and flatness. The results indicate irregular lesions have less elongation and flatness than periapical lesions with a regular shape (Table 6).

**Difference in Radiomic Features according to the Presence of Expansion in the Periapical Lesion**

Of the 100 images, 15 showed expansions of the periapical lesion. These 15 images were matched with 15 that did not show expansion, ensuring a corresponding age range and gender proportion to the patients with expansion (Table 4). No significant differences were found in the radiomic characteristics between the images showing expansion and those without expansion of the periapical lesion (Table 7).

## DISCUSSION

In this study, the volume size of the periapical lesion was significantly correlated with the GNTD contrast parameter and the energy parameter. The results indicate that the larger the lesion's size, the greater the energy and the lower the contrast. An increase in energy may indicate a more aggressive or active lesion, which could help diagnose or predict the lesion. A reduced value in the radiomic parameter NGTDMC correlates with larger lesion sizes and cortical erosion. Finally, the analysis of the shape of periapical lesions and their radiomic characteristics revealed that lesions with a regular shape exhibited greater elongation and flattening.

**TABLE 6.** Difference of the radiomic parameters evaluated according to shape of the periapical lesion

| Parameter | Shape | n | Mean | SD | Test | p |
|---|---|---|---|---|---|---|
| Shape_Elongation | Regular | 33 | 0.794 | 0.115 | Student t | 0.006* |
| | Iregular | 33 | 0.708 | 0.129 | | |
| Shape_Flatness | Regular | 33 | 0.614 | 0.107 | Student t | 0.005* |
| | Iregular | 33 | 0.534 | 0.113 | | |
| Shape_MeshVolume | Regular | 33 | $6.36\times10^{12}$ | $3.66\times10^{13}$ | Mann-Whitney | 0.09 |
| | Iregular | 33 | $4.84\times10^{12}$ | $2.74\times10^{13}$ | | |
| Shape_Sphericity | Regular | 33 | 0.385 | 0.115 | Mann-Whitney | 0.3 |
| | Iregular | 33 | 0.346 | 0.094 | | |
| Firstorder_Energy | Regular | 33 | $1.68\times10^{10}$ | $1.78\times10^{10}$ | Mann-Whitney | 0.1 |
| | Iregular | 33 | $3.13\times10^{10}$ | $4.05\times10^{10}$ | | |
| Firstorder_Entropy | Regular | 33 | 4.932 | 0.307 | Student t | 0.5 |
| | Iregular | 33 | 4.98 | 0.294 | | |
| Firstorder_TotalEnergy | Regular | 33 | $2.89\times10^{9}$ | $8.09\times10^{9}$ | Mann-Whitney | 0.3 |
| | Iregular | 33 | $3.23\times10^{9}$ | $1.04\times10^{10}$ | | |
| Firstorder_Uniformity | Regular | 33 | 0.04 | 0.01 | Mann-Whitney | 0.7 |
| | Iregular | 33 | 0.039 | 0.008 | | |
| Texture_GLCM Contrast | Regular | 33 | 21.405 | 9.83 | Mann-Whitney | 0.9 |
| | Iregular | 33 | 19.995 | 6.216 | | |
| Texture NGTDMC | Regular | 33 | 0.068 | 0.026 | Mann-Whitney | 0.1 |
| | Iregular | 33 | 0.062 | 0.029 | | |

*: p<0.05. n: Number, SD: Standard deviation, GLCM: Grey-level co- occurrence matrix, NGTDMC: Neighbouring grey tone difference matrix contrast

**TABLE 7.** Difference of the radiomic parameters evaluated according to the presence or absence of expansion

| Parameter | Expansion | n | Mean | SD | Test | p |
|---|---|---|---|---|---|---|
| Shape_Elongation | Yes | 15 | 0.77 | 0.16 | Student t | 0.5 |
| | No | 15 | 0.74 | 0.15 | | |
| Shape_Flatness | Yes | 15 | 0.59 | 0.14 | Student t | 0.8 |
| | No | 15 | 0.58 | 0.1 | | |
| Shape_MeshVolume | Yes | 15 | $1.50\times10^{13}$ | $5.61\times10^{13}$ | Mann-Whitney | 0.7 |
| | No | 15 | 25561.46 | 64780.86 | | |
| Shape_Sphericity | Yes | 15 | 0.34 | 0.07 | Mann-Whitney | 0.2 |
| | No | 15 | 0.37 | 0.08 | | |
| Firstorder_Energy | Yes | 15 | $2.36\times10^{10}$ | $1.30\times10^{10}$ | Mann-Whitney | 0.2 |
| | No | 15 | $1.94\times10^{10}$ | $1.86\times10^{10}$ | | |
| Firstorder_Entropy | Yes | 15 | 5.04 | 0.34 | Student t | 0.3 |
| | No | 15 | 5.13 | 0.15 | | |
| Firstorder_TotalEnery | Yes | 15 | $7.50\times10^{9}$ | $1.63\times10^{10}$ | Mann-Whitney | 0.3 |
| | No | 15 | $3.24\times10^{9}$ | $7.64\times10^{9}$ | | |
| Firstorder_Uniformity | Yes | 15 | 0.04 | $8.67\times10^{-3}$ | Mann-Whitney | 0.4 |
| | No | 15 | 0.03 | $4.05\times10^{-3}$ | | |
| Texture_GLCM Contrast | Yes | 15 | 23.22 | 7.88 | Mann-Whitney | 0.3 |
| | No | 15 | 21.25 | 6.92 | | |
| Texture_ NGTDMC | Yes | 15 | 0.07 | 0.02 | Mann-Whitney | 0.5 |
| | No | 15 | 0.07 | 0.03 | | |

n: Number, SD: Standard deviation, GLCM: Grey-level co- occurrence matrix, NGTDMC: Neighbouring grey tone difference matrix contrast

The present study used small field-of-view CBCTs due to their advantages, such as the possibility of a smaller voxel size and higher image resolution. However, it presents challenges such as scattered radiation and artefacts, which affect image quality (16).

The retrospective nature of this study may limit the generalizability of findings, as it relies on existing data rather than controlled prospective collection. Additionally, the study was conducted with a convenience sample, which may not represent the general population more adequately. However, given the absence of previous similar studies, this study can serve as a pilot investigation to inform better sample size calculations for future research. Furthermore, although a semi-automatic segmentation method was utilised for CBCT image analysis, there remains a possibility of human error potentially affecting result accuracy. Despite efforts to standardise image protocols, variability and bias in CBCT image interpretation may still occur.

This study computed sphericity directly using Pyradiomics software, which provides a robust and automated method

for extracting radiomic features from medical images. This contrasts with the approach taken by Boubaris et al. (15), who derived sphericity semi-manually using Excel software by calculating from individual volume values and surface area measurements. The use of Pyradiomics ensures a higher degree of accuracy and reproducibility due to its automated nature and the sophisticated algorithms it employs.

A significant strength of this study is the employment of small field-of-view CBCT scans, known for their enhanced image quality, which results in more precise and accurate measurements. This marked improvement over the large FOV CBCT scans used in previous studies, often associated with lower image resolution and potentially less reliable data. The improved image quality of reduced FOV CBCT scans can lead to more accurate quantification of radiomic features, thereby strengthening the validity of the study's findings. However, the use of reduced FOV CBCT scans, while advantageous in terms of image quality, may be less widely applicable in clinical settings where full FOV scans are more commonly used due to their broader diagnostic capabilities. This could impact the generalizability of the study's findings to real-world clinical practice (17, 18).

According to our results, the volume of the periapical lesion was significantly correlated with the GNTD contrast parameter and the energy parameter. This aligns with the study by Bianchi et al. (19), which reported that variations in energy values could serve as biomarkers in diagnosing temporomandibular joint osteoarthritis. Furthermore, lower GLCM and GNTD contrast have been associated with lesions that tend to cause cortical expansion and thinning. For instance, Jiang et al. (20) found that lower GLCM and GNTD contrast values are related to odontogenic keratocysts, which typically exhibit cortical expansion and thinning compared to simple bone cysts, which have higher GLCM and GNTD contrast values and do not exhibit significant growth or cause cortical expansion and thinning.

A reduced value in the radiomic parameter GNTD contrast correlates with larger lesion sizes and cortical erosion, consistent with previous research highlighting the significance of radiomic texture parameters in differentiating between odontogenic and non-odontogenic sinusitis. In that study, sinus membrane thickening associated with odontogenic sinusitis presented higher grey-level co-occurrence matrix (GLCM) contrast and entropy than that related to non-odontogenic sinusitis (21). These findings align with previous studies that report larger lesions generally have a poorer prognosis (22, 23). Therefore, precise values such as radiomic contrast and energy features can aid in developing more accurate predictive models for the prognosis of periapical lesions (24). In this study, the sphericity and volumetric size of the periapical lesions did not exhibit significant differences, a finding that diverges from the results reported by Boubaris et al. (15), who found that larger periapical lesions exhibited greater sphericity (17).

The analysis of the shapes of periapical lesions and their radiomic characteristics revealed that lesions with a regular shape exhibited greater elongation and flattening. This observation aligns with the findings of similar studies. For instance, Sukegawa et al. (25) analysed the morphology of radicular cysts in 146 patients, reporting that radicular cysts in the maxilla were associated with bone expansion in both the mesiodistal and buccolingual directions. In contrast, those in the mandible progressed mesiodistally without bone expansion.

Regarding the presence or absence of erosion in periapical lesions and their associated radiomic characteristics, significant differences were observed in sphericity (a texture-type feature), texture contrast, and the first-order feature energy. These findings are consistent with prior studies, which suggest that texture features may be the most reliable biomarkers for assessing lesion severity. For example, Kavitha et al. (26) observed that texture features yielded significant findings when using radiomic analysis on panoramic radiographs of Korean females to diagnose and classify osteoporosis in the jaw. Similarly, Kawashima et al. (27) demonstrated the utility of texture features extracted from head tomography scans of 29 patients in diagnosing osteoporosis in different regions of the skull and maxillary bones. Finally, no significant differences were observed between the groups regarding the presence or absence of cortical expansion caused by periapical lesions and the evaluated radiomic characteristics. This may be attributed to the relatively small sample size, with only 15 CBCTs included per group. However, literature exists with similar sample sizes where significant results were obtained. Therefore, it is recommended that future studies incorporate a greater number of radiomic features to identify significant results (28).

Several methods have been reported for enhancing low-quality images used in radiomics. For instance, Khan et al. (29) decomposed images into reflection and illumination components to improve visibility, contrast, and edge preservation. While more precise than manual, semi-automatic segmentation still allows for human error, which can be mitigated by implementing deep learning algorithms. Ekert et al. (30) successfully used a deep convolutional neural network to detect apical lesions, reducing human error. To optimise radiomics, large datasets, standardised procedures, and verification processes are necessary, with existing initiatives aiming to standardise medical practices to support radiomics advancement (31).

Future research includes developing machine learning or artificial intelligence algorithms utilising radiomic parameters to enhance the detection and classification of periapical lesions. Additionally, investigating the impact of different endodontic treatment protocols on the radiomic characteristics of lesions over time could provide valuable insights. Furthermore, comparative studies assessing the utility of radiomics in CBCT against other imaging modalities such as periapical radiography, panoramic radiography, and magnetic resonance imaging would be beneficial. Moreover, exploring the relationship between molecular and genetic biomarkers and radiomic features in periapical lesions could deepen the understanding of these pathologies (32). Other areas of interest involve establishing histological correlations with images analysed by radiomics. Additionally, exploring radiomics as a diagnostic tool for the differential diagnosis between apical lesions and those of non-odontogenic origin could be a promising avenue for research (33).

## CONCLUSION

The recent study found significant differences in radiomic features of periapical lesions. This emphasises the impact of volumetric size, cortical erosion, and shape on various radiomic parameters. The clinical relevance of this research is significant as it has the potential to improve the quantitative characterisation of periapical lesions, leading to an objective interpretation. These findings could be used in machine learning algorithms to automate measurements and predictions based on CBCT images, which could enhance treatment planning, prognosis, differential diagnosis, and risk assessment. However, these insights are preliminary, and further research is necessary to clarify these relationships and their potential clinical implications.

### Disclosures

**Ethics Committee Approval:** The study was approved by the Autonomous University of San Luis Potosí Faculty of Stomatology Ethics Committee (no: CEI-FE-011-022, date: 15/04/2022).

**Authorship Contributions:** Concept – O.L.G.; Design – M.F.S.O.; Data collection and/or processing – N.P.M.; Data analysis and/or interpretation – N.G.M.C.; Critical review – J.T.M.

**Conflict of Interest:** All authors declared no conflict of interest.

**Use of AI for Writing Assistance:** No AI technologies utilized.

**Financial Disclosure:** The authors declared that this study received no financial support.

**Peer-review:** Externally peer-reviewed.

## REFERENCES

1. Petersson A, Axelsson S, Davidson T, Frisk F, Hakeberg M, Kvist T, et al. Radiological diagnosis of periapical bone tissue lesions in endodontics: a systematic review. Int Endod J 2012; 45(9):783–801. [CrossRef]
2. Tomaszewski MR, Gillies RJ. The biological meaning of radiomic features. Radiology 2021; 299(2):E256. [CrossRef]
3. Setzer FC, Lee SM. Radiology in endodontics. Dent Clin North Am 2021; 65(3):475–86. [CrossRef]
4. Gaêta-Araujo H, Nascimento EHL, Brasil DM, Gomes AF, Freitas DQ, De Oliveira-Santos C. Detection of simulated periapical lesion in intraoral digital radiography with different brightness and contrast. Eur Endod J 2019; 4(3):133–8. [CrossRef]
5. Tian J, Dong D, Liu Z, Wei J. Introduction. In: Tian J, Dong D, Liu Z, editors. Radiomics and Its Clinical Application: Artificial Intelligence and Medical Big Data. 1st ed. London: Academic Press; 2021. p. 1–2. [CrossRef]
6. Lambin P, Leijenaar RTH, Deist TM, Peerlings J, de Jong EEC, van Timmeren J, et al. Radiomics: the bridge between medical imaging and personalized medicine. Nat Rev Clin Oncol 2017; 14(12):749–62. [CrossRef]
7. Yip SS, Aerts HJ. Applications and limitations of radiomics. Phys Med Biol 2016; 61(13):R150–66. [CrossRef]
8. Preuss K, Thach N, Liang X, Baine M, Chen J, Zhang C, et al. Using quantitative imaging for personalized medicine in pancreatic cancer: a review of radiomics and deep learning applications. Cancers 2022; 14(7):1654. [CrossRef]
9. Leite AF, Vasconcelos KF, Willems H, Jacobs R. Radiomics and machine learning in oral healthcare. Proteomics Clin Appl 2020; 14(3):e1900040. [CrossRef]
10. Karamifar K, Tondari A, Saghiri MA. Endodontic periapical lesion: an overview on the etiology, diagnosis and current treatment modalities. Eur Endod J 2020; 5(2):54–67. [CrossRef]
11. Ito K, Kurasawa M, Sugimori T, Muraoka H, Hirahara N, Sawada E, et al. Risk assessment of external apical root resorption associated with orthodontic treatment using computed tomography texture analysis. Oral Radiol 2023; 39(1):75–82. [CrossRef]
12. Poswar Fde O, Farias LC, Fraga CA, Bambirra W Jr, Brito-Júnior M, Sousa-Neto MD, et al. Bioinformatics, interaction network analysis, and neural networks to characterize gene expression of radicular cyst and periapical granuloma. J Endod 2015; 41(6):877–83. [CrossRef]
13. Hiraiwa T, Ariji Y, Fukuda M, Kise Y, Nakata K, Katsumata A, et al. A deep-learning artificial intelligence system for assessment of root morphology of the mandibular first molar on panoramic radiography. Dentomaxillofac Radiol 2019; 48(3):20180218. [CrossRef]
14. Shaikh F, Dehmeshki J, Bisdas S, Roettger-Dupont D, Kubassova O, Aziz M, et al. Artificial intelligence-based clinical decision support systems using advanced medical imaging and radiomics. Curr Probl Diagn Radiol 2021; 50(2):262–7. [CrossRef]
15. Boubaris M, Chan KL, Zhao W, Cameron A, Sun J, Love R, et al. A novel volume-based cone-beam computed tomographic periapical index. J Endod 2021; 47(8):1308–13. [CrossRef]
16. Bianchi J, Gonçalves JR, Ruellas ACO, Vimort JB, Yatabe M, Paniagua B, et al. Software comparison to analyze bone radiomics from high resolution CBCT scans of mandibular condyles. Dentomaxillofac Radiol 2019; 48(6):20190049. [CrossRef]
17. Boubaris M, Cameron A, Love R, George R. Sphericity of periapical lesion and its relation to the novel CBCT periapical volume index. J Endod 2022; 48(11):1395–9. [CrossRef]
18. Moskowitz CS, Welch ML, Jacobs MA, Kurland BF, Simpson AL. Radiomic analysis: study design, statistical analysis, and other bias mitigation strategies. Radiology 2022; 304(2):265–73. [CrossRef]
19. Bianchi J, Gonçalves JR, de Oliveira Ruellas AC, Ashman LM, Vimort JB, Yatabe M, et al. Quantitative bone imaging biomarkers to diagnose temporomandibular joint osteoarthritis. Int J Oral Maxillofac Surg 2021; 50(2):227–35. [CrossRef]
20. Jiang ZY, Lan TJ, Cai WX, Tao Q. Primary clinical study of radiomics for diagnosing simple bone cyst of the jaw. Dentomaxillofac Radiol 2021; 50(7):20200384. [CrossRef]
21. Ito K, Kondo T, Andreu-Arasa VC, Li B, Hirahara N, Muraoka H, et al. Quantitative assessment of the maxillary sinusitis using computed tomography texture analysis: odontogenic vs non-odontogenic etiology. Oral Radiol 2022; 38(3):315–24. [CrossRef]
22. Gudac J, Hellén-Halme K, Maciulskiene V. The changes in size of periapical lesions after root canal treatments assessed by digital periapical radiography and cone-beam computed tomography: a 2-years prospective clinical study. Medicina (Kaunas) 2022; 58(10):1437. [CrossRef]
23. van der Borden WG, Wang X, Wu MK, Shemesh H. Area and 3-dimensional volumetric changes of periapical lesions after root canal treatments. J Endod 2013; 39(10):1245–9. [CrossRef]
24. Liu Z, Liu J, Zhou Z, Zhang Q, Wu H, Zhai G, et al. Differential diagnosis of ameloblastoma and odontogenic keratocyst by machine learning of panoramic radiographs. Int J Comput Assist Radiol Surg 2021; 16(3):415–22. [CrossRef]
25. Sukegawa S, Matsuzaki H, Katase N, Kawai H, Kanno T, Asaumi JI, et al. Morphological characteristics of radicular cysts using computed tomography. Odontology 2020; 108(1):74–83. [CrossRef]
26. Kavitha MS, An SY, An CH, Huh KH, Yi WJ, Heo MS, et al. Texture analysis of mandibular cortical bone on digital dental panoramic radiographs for the diagnosis of osteoporosis in Korean women. Oral Surg Oral Med Oral Pathol Oral Radiol 2015; 119(3):346–56. [CrossRef]
27. Kawashima Y, Fujita A, Buch K, Li B, Qureshi MM, Chapman MN, et al. Using texture analysis of head CT images to differentiate osteoporosis from normal bone density. Eur J Radiol 2019; 116:212–8. [CrossRef]
28. De Rosa CS, Bergamini ML, Palmieri M, Sarmento DJS, de Carvalho MO, Ricardo ALF, et al. Differentiation of periapical granuloma from radicular cyst using cone beam computed tomography images texture analysis. Heliyon 2020; 6(10):e05194. [CrossRef]
29. Khan R, Akbar S, Khan A, Marwan M, Qaisar ZH, Mehmood A, et al. Dental image enhancement network for early diagnosis of oral dental disease. Sci Rep 2023; 13(1):5312. [CrossRef]
30. Ekert T, Krois J, Meinhold L, Elhennawy K, Emara R, Golla T, et al. Deep learning for the radiographic detection of apical lesions. J Endod 2019; 45(7):917–22. [CrossRef]
31. The Image Biomarker Standardisation Initiative. Available at: https://github.com/theibsi. Accessed April 27, 2023.
32. Hung KF, Ai QYH, Wong LM, Yeung AWK, Li DTS, Leung YY. Current applications of deep learning and radiomics on CT and CBCT for maxillofacial diseases. Diagnostics (Basel) 2022; 13(1):110. [CrossRef]
33. Orhan K, Driesen L, Shujaat S, Jacobs R, Chai X. Development and validation of a magnetic resonance imaging-based machine learning model for TMJ pathologies. Biomed Res Int 2021; 2021:6656773. [CrossRef]